Stability of helical textures in ^{3}He-A

Alexander L. Fetter
Institute of Theoretical Physics, Physic Department, Stanford University, Stanford, California 94305
(Received 1 February 1979)

In the presence of weak uniform superflow, bulk ^{3}He-A near T_c assumes a uniform texture with $\hat{l}$ parallel to $\vec{v}_s$. Below a characteristic temperature T_h, however, the temperature dependence of the hydrodynamic free energy can induce a helical deformation. The equilibrium configuration of such helices is investigated, using Cross's weak-coupling gas model with Fermi-liquid corrections to evaluate the hydrodynamic parameters. This model predicts $T_h \approx 0.82 T_c$ and that helical textures can be stable at all $T < T_h$ with suitable adjustment of the apex angle and pitch.

I. INTRODUCTION

The discovery that ^{3}He becomes superfluid at $T \approx 2.7$ mK has stimulated extensive theoretical and experimental investigations of this new condensed quantum fluid.[1,2] It differs from the more familiar superfluid ^{4}He II because of the unit angular momenta associated with the p-wave triplet Cooper pairs. These internal degrees of freedom lead to intrinsic anisotropies, most notably in the A phase, where the orbital angular momentum $\hat{l}$ provides a preferred axis. For example, the anisotropy of the superfluid density tends to align $\vec{v}_s$ and $\hat{l}$, and a magnetic field acts through the dipole coupling to align $\hat{l}$ perpendicular to $\vec{H}$. For any given geometry, the final configuration represents a compromise between these and other competing effects, such as the elastic deformation energy associated with slow spatial variations in $\hat{l}$. In particular, recent theoretical studies based on the hydrodynamic free energy have predicted[3–7] a striking hydrodynamic instability, in which the simple uniform texture with $\hat{l}$ parallel to $\vec{v}_s$ undergoes a spontaneous distortion to a helical structure below a critical temperature T_h determined by the hydrodynamic parameters. The present paper examines the stability of this new helical texture with respect to small-amplitude plane-wave perturbations proportional to $e^{i\vec{k}\cdot\vec{r}}$ throughout the domain $T < T_h$.

The general hydrodynamic free energy is discussed in Sec. II, along with the dynamical equations for $\hat{l}$. The equilibrium condition for a static helix is derived in Sec. III, and its stability is analyzed in Sec. IV, both analytically and numerically. Throughout this work, Cross's weak-coupling gas model[8] is used to evaluate the temperature dependence of the hydrodynamic parameters, including the important effect of Fermi-liquid corrections. The Appendix contains some practical details of this calculation.

II. HYDRODYNAMIC FREE ENERGY

In the hydrodynamic model, the order parameter of ^{3}He-A has the form

$$A_{\mu i} = \Delta \hat{d}_\mu (\hat{m} + i\hat{n})_i , \tag{1}$$

where Δ is a temperature-dependent constant, $\hat{d}$ is a unit vector perpendicular to the axis of spin quantization for the Cooper pairs, and $\hat{m}$ and $\hat{n}$ are orthogonal unit vectors with $\hat{l} \equiv \hat{m} \times \hat{n}$ lying along the direction of the Cooper pair's orbital angular momentum. Since the direction of these unit vectors may vary, the order parameter is specified by giving $\hat{d}$, $\hat{m}$, and $\hat{n}$ at every point in space. Spatial variations of $\hat{m}$ and $\hat{n}$ may be further classified into two distinct types, involving rotations about the direction $\hat{l}$ and changes in $\hat{l}$ itself. The former alter the phase of the order parameter and give rise to a superfluid velocity

$$\vec{v}_s = \hat{m}_i \vec{\nabla} \hat{n}_i = \tfrac{1}{2}(\hat{m}_i \vec{\nabla} \hat{n}_i - \hat{n}_i \vec{\nabla} \hat{m}_i) , \tag{2}$$

where a factor $\hbar/2m_3$ has been absorbed to give $\vec{v}_s$ the dimension of a wave number. The latter variations, in contrast, represent an elastic distortion of the $\hat{l}$ vector field, analogous to that of a nematic liquid crystal.[9]

These various spatial variations produce corresponding terms in the hydrodynamic free energy. First, the superfluid velocity leads to a kinetic energy density

$$f_k = \tfrac{1}{2}\vec{v}_s \vec{\rho}_s \vec{v}_s + \vec{v}_s \vec{c}\, \mathrm{curl}\, \hat{l} , \tag{3}$$

where $\vec{\rho}_s$ and $\vec{c}$ are uniaxial tensors of the form

$$\vec{\rho}_s = \rho_s \vec{1} - \rho_0 \hat{l}\hat{l} = \rho_s^{\parallel} \vec{1} + \rho_0 (\vec{1} - \hat{l}\hat{l}) ,$$
$$\vec{c} = c_1 \vec{1} - c_0 \hat{l}\hat{l} \tag{4}$$

and $\rho_s^{\parallel} \equiv \rho_s - \rho_0$. The associated supercurrent

$$\vec{j}_s = \partial f_k / \partial \vec{v}_s \,, \tag{5a}$$

$$\vec{j}_s = \vec{\rho}_s \vec{v}_s + \vec{c}\,\mathrm{curl}\,\hat{l} \,, \tag{5b}$$

contains not only the familiar superfluid term but also one proportional to curl $\hat{l}$, analogous to the contribution curl $\vec{M}$ to the electric current in a magnetic material. Second, the deformations in $\hat{l}$ and $\hat{d}$ lead to an elastic energy[8]

$$\begin{aligned} f_{el} = {} & \tfrac{1}{2}\bar{K}_s(\mathrm{div}\,\hat{l})^2 + \tfrac{1}{2}\bar{K}_t(\hat{l}\cdot\mathrm{curl}\,\hat{l})^2 + \tfrac{1}{2}\bar{K}_b(\hat{l}\times\mathrm{curl}\,\hat{l})^2 + \tfrac{1}{2}K_1(\hat{l}\cdot\vec{\nabla})\hat{d}_\mu(\hat{l}\cdot\vec{\nabla})\hat{d}_\mu \\ & + \tfrac{1}{2}K_2(\hat{l}\times\vec{\nabla})_i\hat{d}_\mu(\hat{l}\times\vec{\nabla})_i\hat{d}_\mu \,, \end{aligned} \tag{6}$$

apart from a total divergence term that does not affect the bulk free energy. Finally, the dipole coupling between $\hat{l}$ and $\hat{d}$ introduces a term of the form

$$f_D = -\tfrac{1}{2}\lambda_D(\hat{d}\cdot\hat{l})^2 \tag{7}$$

and an external magnetic field $\vec{H}$ acts on $\hat{d}$ to give

$$f_M = \tfrac{1}{2}\lambda_M(\vec{H}\cdot\hat{d})^2 \,. \tag{8}$$

The total free energy is the sum of the contributions (3), (6), (7), and (8).

If $\vec{H}=0$ and $\vec{v}_s$ is small, the dipole energy predominates. It is then natural to assume that $\hat{d}$ lies along $\hat{l}$, in which case the elastic energy has the simpler structure

$$\begin{aligned} f_{el} = {} & \tfrac{1}{2}K_s(\mathrm{div}\,\hat{l})^2 + \tfrac{1}{2}K_t(\hat{l}\cdot\mathrm{curl}\,\hat{l})^2 \\ & + \tfrac{1}{2}K_b(\hat{l}\times\mathrm{curl}\,\hat{l})^2 \,, \end{aligned} \tag{9}$$

where K_s, K_t, and K_b have the "dipole-locked" values

$$K_s = \bar{K}_s + K_2 \,, \quad K_t = \bar{K}_t + K_2 \,, \quad K_b = \bar{K}_b + K_1 \,. \tag{10}$$

The present paper will consider only this dipole-locked regime in zero magnetic field, when the total free-energy density becomes

$$f = f_k + f_{el} \,, \tag{11}$$

apart from an additive constant. In this case, the order parameter (1) is equivalent to a rigid orthogonal triad $(\hat{l},\hat{m},\hat{n})$ and requires three parameters to specify its orientation at each point in space. We shall generally take these to be the conventional Euler angles[10] (α,β,γ), in which β and α are the polar and azimuthal angles of the unit vector $\hat{l}$ relative to some fixed coordinate axes and γ represents an additional rotation of $\hat{m}$ and $\hat{n}$ about $\hat{l}$.

An equilibrium configuration is one that minimizes the total free energy, which is obtained as the volume integral of Eq. (11). As in any variational calculation, it is essential to maintain the proper independent variables. Although the Euler angles are known from classical mechanics to provide a suitable set of generalized coordinates for a rigid body, the following physical argument indicates that the present problem in general requires a slightly different choice. Consider an infinitesimal rotation $\delta\vec{\Omega}$ of the triad $\hat{l}$, $\hat{m}$, $\hat{n}$. This rotation may be expressed by its components along the original triad according to

$$\delta\vec{\Omega} = \delta\Phi\hat{l} + \delta\vec{\Omega}_\perp \,, \tag{12}$$

with $\delta\vec{\Omega}_\perp$ the projection onto the plane of $\hat{m}$ and $\hat{n}$. These two terms are physically quite distinct: $\delta\vec{\Omega}_\perp$ changes the direction of $\hat{l}$ by an amount $\delta\hat{l} = \delta\vec{\Omega}_\perp \times \hat{l}$; it leads to a restoring force with an orbital viscosity μ.[11] On the other hand $\delta\Phi$ is merely an infinitesimal rotation about $\hat{l}$ with no restoring force. Thus the dynamical equations for the order parameter separate into two parts[12]: one involving the motion of $\hat{l}$ without rotation

$$\mu\hat{l}\times\frac{\partial\hat{l}}{\partial t} = -\hat{l}\times\frac{\delta f}{\delta\hat{l}}\bigg|_{\delta\Phi=0} \tag{13a}$$

and the other involving a rotation about the fixed direction $\hat{l}$

$$0 = -\frac{\delta f}{\delta\Phi}\bigg|_{\delta\hat{l}=0} \,. \tag{13b}$$

To interpret these expressions, it is useful to express the unit vectors in terms of the Euler angles

$$\hat{l} = \hat{x}\sin\beta\cos\alpha + \hat{y}\sin\beta\sin\alpha + \hat{z}\cos\beta \,, \tag{14a}$$

$$\hat{m} = \hat{m}_1\cos\gamma + \hat{n}_1\sin\gamma \,, \tag{14b}$$

$$\hat{n} = -\hat{m}_1\sin\gamma + n_1\cos\gamma \,, \tag{14c}$$

where the auxiliary quantities $\hat{m}_1$ and $\hat{n}_1$ are given by

$$\hat{m}_1 = \hat{x}\cos\beta\cos\alpha + \hat{y}\cos\beta\sin\alpha - \hat{z}\sin\beta \,, \tag{15a}$$

$$\hat{n}_1 = -\hat{x}\sin\alpha + \hat{y}\cos\alpha \,. \tag{15b}$$

Under an infinitesimal rotation characterized by small changes $\delta\alpha$, $\delta\beta$, and $\delta\gamma$ in the Euler angles, it is easy to verify that

$$\delta\Phi = \cos\beta\delta\alpha + \delta\gamma \,, \tag{16a}$$

$$\delta\vec{\Omega}_\perp = -\sin\beta\delta\alpha\hat{m}_1 + \delta\beta\hat{n}_1 \,. \tag{16b}$$

As expected, $\delta\alpha$ and $\delta\beta$ wholly characterize the infinitesimal change in $\hat{l}$, but $\delta\Phi$ differs from $\delta\gamma$ by the projection of $\hat{z}\,\delta\alpha$ onto $\hat{l}$. This latter dependence may be handled as follows: If the free-energy density is

considered a function of the Euler angles and their gradients, then the variation in the total free energy may be expressed in the usual form

$$\delta\int d^3r f=\int d^3r\left[\delta\alpha\left(\frac{\delta f}{\delta\alpha}\right)_{\beta\gamma}+\delta\beta\left(\frac{\delta f}{\delta\beta}\right)_{\alpha\gamma}+\delta\gamma\left(\frac{\delta f}{\delta\gamma}\right)_{\alpha\beta}\right], \tag{17}$$

where for example,

$$\left(\frac{\delta f}{\delta\gamma}\right)_{\alpha\beta}\equiv\frac{\partial f}{\partial\gamma}-\vec{\nabla}\cdot\left(\frac{\partial f}{\partial\vec{\nabla}\gamma}\right), \tag{18}$$

and the partial derivatives are taken keeping fixed the remaining variables of the set $(\alpha,\vec{\nabla}\alpha,\beta,\vec{\nabla}\beta,\gamma,\vec{\nabla}\gamma)$. Equation (16a) relates $\delta\gamma$ to the independent variations $\delta\alpha$ and $\delta\Phi$, and substitution into Eq. (17) gives an expression of the form

$$\delta\int d^3r f=\int d^3r\left[\delta\alpha\left(\frac{\delta f}{\delta\alpha}\right)_{\beta\Phi}+\delta\beta\left(\frac{\delta f}{\delta\beta}\right)_{\alpha\Phi}+\delta\Phi\left(\frac{\delta f}{\delta\Phi}\right)_{\alpha\beta}\right], \tag{19}$$

where the coefficients are given by

$$\left(\frac{\delta f}{\delta\alpha}\right)_{\beta\Phi}=\left(\frac{\delta f}{\delta\alpha}\right)_{\beta\gamma}-\cos\beta\left(\frac{\delta f}{\delta\gamma}\right)_{\alpha\beta},$$
$$\left(\frac{\delta f}{\delta\beta}\right)_{\alpha\Phi}=\left(\frac{\delta f}{\delta\beta}\right)_{\alpha\gamma},\quad\left(\frac{\delta f}{\delta\Phi}\right)_{\alpha\beta}=\left(\frac{\delta f}{\delta\gamma}\right)_{\alpha\beta}. \tag{20}$$

The general dynamical equations (13) expressed in terms of the independent variations $\delta\alpha$, $\delta\beta$, and $\delta\Phi$ may now be rewritten in terms of partial derivatives of f with respect to the Euler angles α, β, and γ

$$\mu\sin^2\beta\frac{\partial\alpha}{\partial t}=-\left(\frac{\delta f}{\delta\alpha}\right)_{\beta\Phi}=-\left(\frac{\delta f}{\delta\alpha}\right)_{\beta\gamma}, \tag{21a}$$

$$\mu\frac{\partial\beta}{\partial t}=-\left(\frac{\delta f}{\delta\beta}\right)_{\alpha\Phi}=-\left(\frac{\delta f}{\delta\beta}\right)_{\alpha\gamma}, \tag{21b}$$

$$0=-\left(\frac{\delta f}{\delta\Phi}\right)_{\alpha\beta}=-\left(\frac{\delta f}{\delta\gamma}\right)_{\alpha\beta}. \tag{21c}$$

Here, the right-hand side of Eq. (21a) has been simplified with Eq. (21c). These relations make it evident that the Euler angles themselves turn out to provide a suitable basis for the present calculation, even though the variation $\delta\gamma$ has a less direct interpretation than the variation $\delta\Phi$ in Eq. (16a).

To proceed further, it is necessary to express f directly in terms of the Euler angles. The terms involving $\hat{l}$ and its spatial derivatives follow directly from Eq. (14a), and use of Eq. (2) readily yields the remaining quantity

$$\vec{v}_s=-\cos\beta\vec{\nabla}\alpha-\vec{\nabla}\gamma. \tag{22}$$

Note that neither $\vec{v}_s$ nor $\hat{l}$ contains γ, which is therefore a cyclic variable. As a result, Eqs. (18) and (21c) reduce to the simpler relation

$$\vec{\nabla}\cdot\left(\frac{\partial f}{\partial\vec{\nabla}\gamma}\right)_{\alpha\beta}=0. \tag{23}$$

For some purposes, it is preferable to adopt a slightly different approach that exploits the explicit dependence of f_k on $\vec{v}_s$ and $\hat{l}$, evaluating the partial derivatives in Eq. (21) with the chain rule. A straightforward calculation with Eq. (5a) yields the equivalent dynamical equations

$$\mu\sin^2\beta\frac{\partial\alpha}{\partial t}=\vec{\nabla}\cdot\left(\frac{\partial f}{\partial\vec{\nabla}\alpha}\right)_{\vec{v}_s}-\left(\frac{\partial f}{\partial\alpha}\right)_{\vec{v}_s}+\sin\beta\vec{j}_s\cdot\vec{\nabla}\beta, \tag{24a}$$

$$\mu\frac{\partial\beta}{\partial t}=\vec{\nabla}\cdot\left(\frac{\partial f}{\partial\vec{\nabla}\beta}\right)_{\vec{v}_s}-\left(\frac{\partial f}{\partial\beta}\right)_{\vec{v}_s}-\sin\beta\vec{j}_s\cdot\vec{\nabla}\alpha, \tag{24b}$$

$$0=\vec{\nabla}\cdot\vec{j}_s, \tag{24c}$$

where, as indicated, the partial derivatives are now taken at constant $\vec{v}_s$. Here, the third equation makes explicit the expected conservation of current, which has been used to simplify the last term in Eq. (24a).

These general equations determine the space and time dependence of an arbitrary dipole-locked texture. Unfortunately, they are very complicated, and most analyses have considered only the stability of static textures with respect to small deformations. In that case, Eqs. (24) are linearized in the small deviations from equilibrium, and stability requires that the resulting time dependence is an exponential decay. Equivalently, the small change in the free energy must be positive definite.

III. EQUILIBRIUM HELICAL TEXTURES

The preceding formalism will now be applied to the particular geometry of uniform superflow with $\vec{v}_s=w\hat{z}$ and $\vec{v}_n=0$. This configuration may be considered a model for superflow in a large torus with stationary walls. Bhattacharyya, Ho, and Mermin[3] have shown that the uniform texture $\hat{l}=\hat{z}$ is stable with respect to small perturbations if $\rho_0K_b>(c_0+\frac{1}{2}\rho_s^{\parallel})^2$; this condition exemplifies the qualitative arguments from Sec. I that large anisotropy ρ_0 and bending constant K_b

favor the uniform configuration. When $\rho_0 K_b - (c_0 + \frac{1}{2}\rho_s^{\parallel})^2$ changes sign, however, an instability appears with wave number

$$|k_z| = w(c_0 + \tfrac{1}{2}\rho_s^{\parallel})/K_b \ .$$

Subsequent work[6,7] showed that this instability signaled not a catastrophic collapse but rather a displacive transition to a helical texture. Furthermore, the resulting helix has been shown to remain stable in two distinct cases:

(a) If ρ_0 is only slightly less than the critical value

$$\rho_{0h} \equiv (c_0 + \tfrac{1}{2}\rho_s^{\parallel})^2/K_b \ , \tag{25}$$

it is always possible to find helical textures that are stable with respect to arbitrary perturbations of the form $e^{i\vec{k}\cdot\vec{r}}$.

(b) If all the hydrodynamic parameters retain their weak-coupling Ginzburg-Landau ratios, except $\rho_0/\rho_s^{\parallel}$, which is assumed to decrease monotonically from 1 to 0, then for all $\rho_0/\rho_s^{\parallel}$, helical textures can again be found that are stable with respect to restricted perturbations of the form $\exp(ik_z z)$. As shown in the Appendix, this *generalized Ginzburg-Landau* model is not a particularly good representation of the actual temperature dependence of the hydrodynamic parameters, and it cannot provide more than a qualitative description of the stability.

In contrast to these earlier investigations, the present work studies the stability of helical textures for all accessible temperatures ($0.6T_c \lesssim T \lesssim T_c$) and with respect to arbitrary plane-wave perturbations $e^{i\vec{k}\cdot\vec{r}}$. It is convenient to start with a uniform texture $\hat{l} \| \vec{v}_s$ in a uniform superflow $\vec{v}_s = w\hat{z}$. In this case $\beta = 0$, and the remaining Euler angles α and γ both increase linearly with z

$$\alpha = -uz \ , \quad \gamma = -sz \ , \tag{26}$$

where the minus signs have been introduced to simplify later expressions. Here the constants u and s are fixed by the condition of single valuedness around the large torus; more precisely, if L is the circumference of the torus, then u and s must both be integral multiples of $2\pi/L$. In addition, Eq. (22) shows that the magnitude w of the superflow is also quantized for this uniform texture, with the value

$$w = u + s \ . \tag{27}$$

Near T_c, the weak-coupling dipole-locked values of the hydrodynamic parameters imply that the uniform state is indeed stable. This situation changes with decreasing temperature, however, and as T passes below a critical temperature T_h, a helical texture gradually develops. Let β_0 be the apex angle of this helix at some fixed temperature $T < T_h$. Since u and s are both quantized, they retain the values that they had at T_h and the superfluid velocity becomes

$$\vec{v}_s = v_0 \hat{z} \ , \tag{28a}$$

where

$$v_0 = u\cos\beta_0 + s = w - u(1 - \cos\beta_0) \ . \tag{28b}$$

Note that $\vec{v}_s$ remains uniform and along the original direction. Its magnitude is no longer quantized, however, and can differ by arbitrarily large amounts from the original w, depending on the magnitude and sign of u.[3]

Another physical quantity of interest is the equilibrium supercurrent $\vec{j}_s$, which involves not only $\vec{v}_s$ but also $\mathrm{curl}\hat{l}$. Use of Eq. (14a) immediately gives

$$\mathrm{curl}\hat{l} = u\sin\beta_0(\hat{x}\cos uz - \hat{y}\sin uz) = u\hat{l}_\perp \ , \tag{29}$$

where

$$\hat{l}_\perp = \sin\beta_0(\hat{x}\cos uz - \hat{y}\sin uz)$$

is the projection of $\hat{l}$ onto the x-y plane. In addition, $\hat{l}\cdot\mathrm{curl}\hat{l}$ is just $u\sin^2\beta_0$. Equation (5) shows that the total supercurrent $\vec{j}_{s0}$ not only has a uniform axial component

$$(\vec{j}_{s0})_z = v_0(\rho_s^{\parallel} + \rho_0\sin^2\beta_0) - c_0 u\cos\beta_0\sin^2\beta_0 \ , \tag{30a}$$

but also a helical component in the x-y plane

$$(\vec{j}_{s0})_\perp = [-v_0\rho_0\cos\beta_0 + u(c - c_0\sin^2\beta_0)]\hat{l}_\perp \ . \tag{30b}$$

Evidently, $\vec{j}_{s0}$ is solenoidal, as required by Eq. (24c).

It is now straightforward to evaluate the free-energy density for the helical texture. The kinetic and elastic contributions become

$$f_k = \tfrac{1}{2}v_0^2(\rho_s^{\parallel} + \rho_0\sin^2\beta_0) - v_0 u c_0\cos\beta_0\sin^2\beta_0 \ , \tag{31a}$$

$$f_{el} = \tfrac{1}{2}u^2\sin^2\beta_0(K_b\cos^2\beta_0 + K_t\sin^2\beta_0) \ , \tag{31b}$$

with v_0 given in Eq. (28b). As a result, the total free-energy density for a static helix has the form

$$f_0 = \tfrac{1}{2}[w - u(1-\cos\beta_0)]^2(\rho_s^{\parallel} + \rho_0\sin^2\beta_0) - [w - u(1-\cos\beta_0)]uc_0\cos\beta_0\sin^2\beta_0 + \tfrac{1}{2}u^2(K_b\sin^2\beta_0\cos^2\beta_0 + K_t\sin^4\beta_0) \ . \tag{32}$$

For given values of the hydrodynamic parameters and fixed w and u, f_0 must be minimized with respect to the remaining variable β_0. This calculation leads to the requirement that a product of two factors must vanish. Thus we demand that β_0 satisfy either

of two equilibrium conditions:

$$\sin\beta_0 = 0 \tag{33}$$

$$[w-u(1-\cos\beta_0)]^2\rho_0\cos\beta_0-[w-u(1-\cos\beta_0)]u[\rho_s^{\parallel}+2c_0+(\rho_0-3c_0)\sin^2\beta_0] + u^2\cos\beta_0[K_b+(2K_t-2K_b+c_0)\sin^2\beta_0]=0\ . \tag{34}$$

The first solution $\sin\beta_0=0$ is just the uniform texture: it always represents a possible static configuration. For certain values of u and the hydrodynamic parameters, however, Eq. (34) provides new helical solutions, which will be analyzed in detail below.

In the original uniform texture ($\beta_0=0$), there are no barriers for transitions between states with different u because the free energy in Eq. (32) is independent of u. Hence only the superfluid velocity $w=u+s$ remains quantized. For $\beta_0\neq 0$, however, f_0 becomes a quadratic form in u, and u presumably takes on the quantized value $u_{\min}$ that minimizes the free energy at the point where β_0 first differs from 0. Direct differentiation of Eq. (32) for fixed nonzero β_0 gives the result

$$u_{\min}=\frac{w[c_0\cos\beta_0(1+\cos\beta_0)+\rho_s^{\parallel}+\rho_0\sin^2\beta_0]}{(K_b\cos^2\beta_0+K_t\sin^2\beta_0)(1+\cos\beta_0)+2c_0\cos\beta_0\sin^2\beta_0+(\rho_s^{\parallel}+\rho_0\sin^2\beta_0)(1-\cos\beta_0)}\ . \tag{35}$$

Suppose that the sample is cooled at fixed pressure from the normal phase into the A phase. Since $T_c > T_h$, only the uniform state ($\beta_0=0$) occurs until Eq. (34) first has a solution at the transition temperature T_h. A general analysis for arbitrary $T<T_h$ and u would be prohibitive, but an expansion of Eq. (34) for $T_h-T \ll T_h$ readily yields the expression

$$\beta_0^2\approx\frac{K_b(c_0+\frac{1}{2}\rho_s^{\parallel})}{(2K_t-\frac{1}{2}\rho_s^{\parallel})(c_0+\frac{1}{2}\rho_s^{\parallel})-\frac{3}{2}K_b\rho_s^{\parallel}} \times\left[\frac{\rho_{0h}-\rho_0}{\rho_{0h}}-\left(\frac{u-u_h}{u_h}\right)^2\right], \tag{36}$$

where

$$\rho_{0h}\equiv[(c_0+\tfrac{1}{2}\rho_s^{\parallel})^2/K_b]_{T_h}\ , \tag{37a}$$

$$u_h=w[(c_0+\tfrac{1}{2}\rho_s^{\parallel})/K_b]_{T_h} \tag{37b}$$

and the equation

$$\rho_0(T_h)=\rho_{0h} \tag{38}$$

determines the T_h. The hydrodynamic parameters in the coefficient of Eq. (36) should be evaluated at the temperature T_h, but its order of magnitude may be estimated as $\frac{5}{4}$ by using the weak-coupling Ginzburg-Landau values because strong-coupling effects are thought to be small.[13] Note that small-angle helices can be in static equilibrium for a range of parameters

$$\left(\frac{u-u_h}{u_h}\right)^2\leq\frac{\rho_{0h}-\rho_0}{\rho_{0h}}\ll 1\ , \tag{39}$$

which determines a parabolic region in the $u-\rho_0$ or $u-T$ plane.

It is evident from Eq. (35) that $u_h=u_{\min}$ in the limit $\beta_0\to 0$ and $T\to T_h$. For lower temperatures, however, u retains the quantized value u_h, but this value in general differs from $u_{\min}$. An expansion of Eq. (35) for small β_0 gives

$$u_{\min}\approx\frac{w(c_0+\frac{1}{2}\rho_s^{\parallel})}{K_b}\left[1-\beta_0^2\left(\frac{K_t+c_0+\frac{1}{4}\rho_s^{\parallel}}{K_b}-\frac{1}{2}-\frac{\rho_0+\frac{3}{4}\rho_s^{\parallel}}{2c_0+\rho_s^{\parallel}}\right)\right], \tag{40}$$

and, as a qualitative estimate, the weak-coupling Ginzburg-Landau values yield $\frac{5}{12}$ for the coefficient of β_0^2. Note that the solution to Eq. (35) depends on temperature through the hydrodynamic parameters; thus any subsequent change in the temperature at fixed quantized u means that u no longer minimizes the free energy. Consequently, a complete analysis of the equilibrium configurations should involve not only a range of T but also values of u far from $u_{\min}$.

To investigate the static equilibrium of such helical structures, the Cross weak-coupling gas model has been used to evaluate the hydrodynamic parameters for all $T\leq T_c$, including Fermi-liquid corrections. The Appendix describes the procedure and the principal numerical conclusions. In particular, these calculations predict the value $T_h\approx 0.82\,T_c$ as the temperature at which small-angle helices first appear. Furthermore, the corresponding critical values of Eq. (37) are

$$\left.\begin{aligned}\rho_{0h}&\approx 1.147\rho_s^{\parallel}\\ u_h&\approx 0.721\,w\end{aligned}\right\}\ \text{at}\ T=T_h\approx 0.82\,T_c\ . \tag{41}$$

It is also interesting to compare these values with those of the generalized Ginzburg-Landau model,[7] which allows $\rho_0/\rho_s^{\parallel}$ to vary between 0 and 1, keeping

the remaining parameters fixed at the dipole-locked ratios

$$c_0=\rho_s^{\parallel}\,,\quad K_s=K_t=K_b=2.5\rho_s^{\parallel}\,. \tag{42}$$

Such a model cannot fix the onset temperature T_h, but it predicts $\rho_{0h}/\rho_s^{\parallel}=0.9$ and $u_h=0.6w$, both of which differ appreciably from the values in Eq. (41).

Since u will not generally minimize the free energy, the equilibrium configuration of the helix is determined solely by Eq. (34). Given the temperature-dependent hydrodynamic parameters, this relation determines a surface in the three-dimensional space with axes u, β_0, and T. In addition, Eq. (34) is quadratic in u, so that a given value of β_0 and T corresponds to at most two values of u. Figure 1 exhibits this surface evaluated with the weak-coupling gas model including Fermi-liquid corrections for the dipole-locked bending constants. Also shown are the intersections with planes of constant T and constant u. For $T>T_h\approx 0.82T_c$, only large-angle helices can occur; in the interval $0.63T_c\lesssim T<T_h$, small-angle helices also can occur, but a forbidden range of intermediate β_0 remains. Below $T\approx 0.63T_c$, in contrast, equilibrium helices can occur for all β_0 by suitably adjusting u. It should be noted that this situation is quite different from that predicted by the generalized Ginzburg-Landau model, when a forbidden region of intermediate β_0 persists for all positive $\rho_0/\rho_s^{\parallel}$.[7]

In any physical situation, the value of u will be set by the initial conditions, and subsequent changes in the temperature will maintain that value of u. Thus the actual form of the helix will be determined by the intersection of this surface with a plane $u=$const.

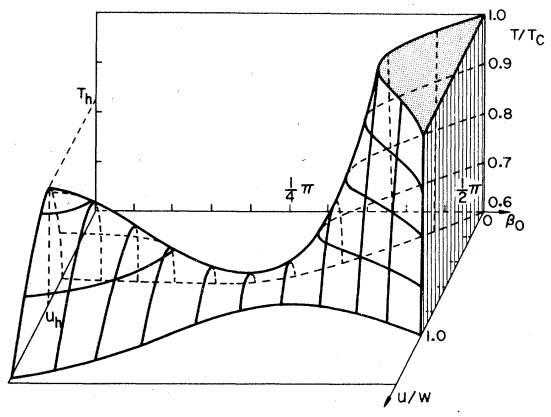

FIG. 1. Surface of static equilibrium helical configurations for ^{3}He-A in zero magnetic field evaluated from Eq. (34) with the temperature-dependent dipole-locked hydrodynamic parameters from Figs. 3, 4, and 6, including Fermi-liquid corrections. Here $2\pi/u$ is the spatial period of the helix and β_0 is the apex angle. Also shown is the intersection with the planes $T/T_c=1.0$, 0.9, 0.8, 0.7, and 0.6, and the planes $2\beta_0/\pi=0,0.1,0.2,\ldots,0.9,1.0$.

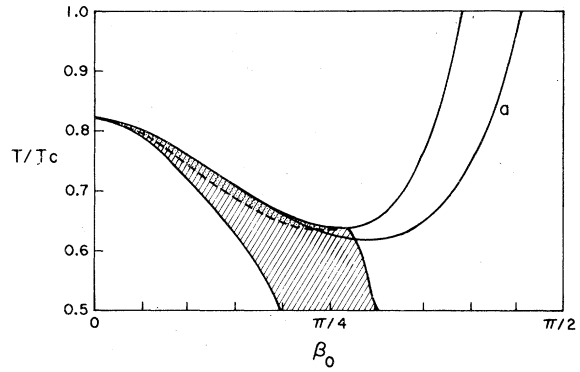

FIG. 2. Projection of the three-dimensional surface from Fig. 1 onto the β_0-T plane. The region of stability (shown shaded) extends just over the ridge and slightly down the far side. Also shown (curve a) is the projection of the intersection with the plane $u=u_h\approx 0.721w$ corresponding to the minimum free energy at the transition temperature T_h.

As a specific example, consider the intersection with the plane corresponding to the critical value $u=u_h=0.721w$ at T_h; for small β_0, the curve (labeled a in Fig. 2) runs very near the "ridge" until $\beta_0\approx 0.7$, when it moves onto the near side of the surface shown in Fig. 1.

The preceding discussion has considered only the condition for static equilibrium, with no reference to stability. Since not all of these equilibrium configurations are expected to be stable, it is essential to analyze the dynamics of various small deformations about the helical structure. This investigation, which is presented in Sec. IV, confirms that helices are stable only in a limited region of the surface in Fig. 1. Nevertheless, the domain of stability extends to all temperatures below T_h, so that stable helices could in principle be found for $T<T_h$ with appropriate adjustment of the initial parameters.

IV. STABILITY OF HELICAL TEXTURES

As discussed in Sec. III, helical textures in ^{3}He-A may be characterized by the Euler angles $\alpha_0=-uz$, $\beta_0=$const, and $\gamma_0=-sz$. The stability of such a configuration may be investigated by considering the small distortions of the helix. These variations can be parameterized by the local changes in the Euler angles $\delta\alpha$, $\delta\beta$, and $\delta\gamma$, but it is preferable to use the related but more physical set [see Eq. (16)] $\delta\alpha,\delta\beta$, which together characterize the change $\delta\hat{l}$ in $\hat{l}$, and the rotation $\delta\Phi=\cos\beta\delta\alpha+\delta\gamma$ about $\hat{l}$. Equivalently, $\delta\gamma$ may be written $\delta\Phi-\cos\beta\delta\alpha$, and an expansion of Eq. (22) to second order yields the corresponding superfluid velocity

$$\vec{v}_s=\vec{v}_{s0}+\delta\vec{v}_s\,, \tag{43}$$

where [see Eq. (28)]

$$\vec{\nabla}_{s0} = v_0\hat{z} = [w - u(1-\cos\beta_0)]\hat{z} \tag{44a}$$

and

$$\delta\vec{v}_s = -u\hat{z}[\sin\beta_0\delta\beta + \tfrac{1}{2}\cos\beta_0(\delta\beta)^2] - \sin\beta_0\delta\alpha\vec{\nabla}\delta\beta - \vec{\nabla}\delta\Phi\ . \tag{44b}$$

Together with the relations $\alpha = \alpha_0 + \delta\alpha$ and $\beta = \beta_0 + \delta\beta$, these expressions suffice to evaluate the free energy through second order in $\delta\alpha$, $\delta\beta$, and $\delta\Phi$.

To proceed further, it is helpful to expand the small variations in Fourier series

$$\delta\alpha(\vec{r}) = V^{-1/2}\sum_{\vec{k}} e^{i\vec{k}\cdot\vec{r}}\delta\alpha_{\vec{k}}\ , \tag{45}$$

with similar series for $\delta\beta$ and $\delta\gamma$. Here V is the quantization volume, the allowed wave numbers $\vec{k}$ are determined by periodic boundary conditions, and reality requires that $\delta\alpha_{\vec{k}}^* = \delta\alpha_{-\vec{k}}$. Since the helical texture is invariant under translations in the x-y plane, modes with different transverse wave vectors are expected to uncouple; in contrast, the periodicity along z with axial wave number u mixes modes with k_z differing by integral multiples of u. An expansion to second order gives the following form for the integrated free energy:

$$F = \int d^3r\, f = F_0 + \delta F\ , \tag{46}$$

where the zero-order term is just V times f_0 given in Eq. (32). The remaining contribution δF contains terms of second order in the small variations as well as a single first-order term proportional to $\delta\beta_{\vec{k}=0}$ (note that u, β_0, and s are here explicitly fixed by the equilibrium configuration). The coefficient of this linear term is just $(\partial f_0/\partial\beta_0)_{w,u}$, so that it vanishes not only for the trivial case of $\beta_0 = 0$ [see Eq. (33)] but also for the equilibrium helical texture [see Eq. (34)] determined by the hydrodynamic parameters and the topological constants w and u. As a result, only the second-order terms remain, and a lengthy analysis eventually leads to an expression of the form

$$\delta F = \sum_{\vec{k}\,\vec{k}'} \delta\Psi_{\vec{k}}^{\dagger} F_{\vec{k}\,\vec{k}'}\delta\Psi_{\vec{k}'}\ , \tag{47}$$

where $\delta\Psi_{\vec{k}}$ is a three-component column vector with elements $\delta\alpha_{\vec{k}}$, $\delta\beta_{\vec{k}}$, and $\delta\Phi_{\vec{k}}$. In addition $F_{\vec{k}\,\vec{k}'}$ is a 3×3 Hermitian matrix with nonzero elements for $\vec{k}' = \vec{k}$, $\vec{k}\pm\vec{u}$ and $\vec{k}\pm 2u$, where $\vec{u} = u\hat{z}$. This particular off-diagonal structure reflects the presence of second spatial derivatives in the free energy. The exact form of $F_{\vec{k}\,\vec{k}'}$ is very complicated, but it has several notable features.

(i) The coupling among wave numbers $\vec{k}$, $\vec{k}\pm\vec{u}$, and $\vec{k}\pm 2\vec{u}$ makes explicit the effect of the spatial periodicity along the z axis. A detailed examination shows that the elements $F_{\vec{k},\vec{k}\mp\vec{u}}$ are proportional to $q_\pm \equiv q_x \pm iq_y$, and that $F_{\vec{k},\vec{k}\mp 2\vec{u}}$ is proportional to $q_\pm^2$, where $\vec{q}$ is the projection of $\vec{k}$ onto the x-y plane. Thus the coupling of commensurate wave vectors occurs only for $\vec{q}\neq 0$ and is wholly omitted in treatments restricted to perturbations of the form $\exp(ik_z z)$.

(ii) Since $F_{\vec{k}\,\vec{k}'}$ is Hermitian, all of its eigenvalues are real. A stable helical structure requires that these eigenvalues also be positive for every $\vec{k}$, ensuring that δF is a positive-definite quadratic form.

(iii) It is sometimes preferable to consider the linearized dynamical equations of motion obtained from Eqs. (13) and (47). The solutions necessarily have an exponential time dependence of the form $\exp(-\sigma t)$, and the corresponding amplitudes satisfy coupled equations

$$\sigma\mu M\delta\Psi_{\vec{k}} = \sum_{\vec{k}'} F_{\vec{k}\,\vec{k}'}\delta\Psi_{\vec{k}'}\ , \tag{48}$$

where M is a diagonal matrix with elements $\sin^2\beta_0$, 1, and 0. This problem is formally identical with that of a coupled mechanical system undergoing small oscillations[14] with a mass matrix μM and a potential matrix F. As in that case, the quantity σ is just the corresponding (real) eigenvalue, and stability here requires that $\sigma > 0$ for all $\vec{k}$. Note that this linearized description can never lead to oscillatory behavior, because the dynamical equations are first order in the time derivatives. Thus any periodic time dependence[15] can arise only from nonlinear contributions[4] or from a more general form for the dynamics.

Before considering the solution of these equations for a general apex angle β, it is helpful to briefly study the limiting behavior for $T \approx T_h$ and small β_0. In this case, the appropriate linear combination of variables is expected to be the same as in the uniform state

$$\delta l_x \pm i\delta l_y = \sin\beta e^{\pm i\alpha} - \sin\beta_0 e^{\pm i\alpha_0} \approx e^{\mp iuz}(\delta\beta \pm i\beta_0\delta\alpha)\ .$$

If only the leading contributions for $\beta_0 \to 0$ are kept, the equation for the variation in the phase variable may be written

$$\delta\Phi_{\vec{k}} = (\rho_s^{\parallel}k_z^2 + \rho_s q^2)^{-1}[-\tfrac{1}{2}iq_-(\rho_0 v_0 + c_0 k_z)(\delta\beta_{\vec{k}+\vec{u}} + i\beta_0\delta\alpha_{\vec{k}+\vec{u}}) - \tfrac{1}{2}iq_+(\rho_0 v_0 - c_0 k_z)(\delta\beta_{\vec{k}-\vec{u}} - i\beta_0\delta\alpha_{\vec{k}-\vec{u}})]\ . \tag{49}$$

This relation shows that $\delta\Phi_{\vec{k}}$ for small β_0 couples only to the modes with $\vec{k} \pm \vec{u}$. Furthermore, the equilibrium condition (36) requires that $u \approx u_h$, and substitution of Eq. (49) into the dynamical equations for $\delta\alpha_{\vec{k}}$ and $\delta\beta_{\vec{k}}$ reduces them to coupled equations for $\delta\beta_{\vec{k}\pm\vec{u}} \pm i\beta_0\delta\alpha_{\vec{k}\pm\vec{u}}$. The associated eigenvalue condition for σ turns out to be the same as in the uniform texture,[3,6] which indicates that the helical state with $\beta_0 \to 0$ and the uniform state are both marginally stable at T_h. In particular, this marginal stability with $\sigma = 0$ occurs for $\vec{k}$ along $\hat{z}$ and $\vec{q} = 0$.

The behavior just below T_h requires the inclusion of correction terms of order β_0^2. An approximate analytical treatment of this small-β_0 regime has already been reported[6] and will be mentioned briefly below. Since it encounters the same difficulties that arise from arbitrary β_0, it is first preferable to treat the general situation.

The off-diagonal elements of F in Eq. (48) lead to an infinite set of linear equations for the coupled amplitudes. This structure requires the use of some approximation scheme, and the existence of a variational basis for Eq. (48) suggests a truncation that retains only a finite number of amplitudes. The simplest approximation keeps only $\delta\Phi_{\vec{k}}$, $\delta\alpha_{\vec{k}}$, and $\delta\beta_{\vec{k}}$; it should be suitable for modes with small q^2, for, as noted previously, the coupling to modes with $\vec{k} \pm \vec{u}$ and $\vec{k} \pm 2\vec{u}$ vanishes at $\vec{q} = 0$. In addition, the onset of instability for the uniform state occurs for $\vec{q} = 0$,[3,6] so that this variational approximation may be expected to include the most important modes for determining the stability of the helical texture. For small β_0, an expansion of the resulting truncated dynamical equations predicts[6] that the system is stable for

$$\left(\frac{u - u_h}{u_h}\right)^2 \leq \frac{1}{3}\left(\frac{\rho_{0h} - \rho_0}{\rho_{0h}}\right) \ll 1 . \tag{50}$$

This range of u is more restrictive than that for static equilibrium given in Eq. (39). When the stability condition (50) is just violated, the instability of the helix occurs at long wavelengths with $\vec{q} = 0$ and $\vec{k}$ along $\hat{z}$. If the helix is prepared with u having the value u_h corresponding to the instability temperature T_h, then Eq. (50) shows that it will remain stable for small $T_h - T$, because of the quantization condition on u.

The same approximation of retaining only the amplitudes $\delta\Phi_{\vec{k}}$, $\delta\alpha_{\vec{k}}$, and $\delta\beta_{\vec{k}}$ has also been studied numerically at all $T < T_h$, using the weak-coupling hydrodynamic parameters from the Appendix. As in the case of a uniform texture,[6] the stability condition becomes a quadratic form P in k^2, with coefficients that depend on the polar angle $\arctan(q/k_z)$ of k with respect to $\hat{z}$. These coefficients also depend on the equilibrium parameters of the helix, which necessarily lie on the surface shown in Fig. 1. For each T, I first set $\vec{q} = 0$ and determined the points on this surface where P vanishes for small k_z ($\ll w$). I then systematically increased k_z and q, which always turned out to make P positive. Consequently, the boundary of stability is again determined by long-wavelength perturbations with $\vec{q} = 0$ and k along $\hat{z}$. The corresponding normal modes of the helix involve a torsional motion at fixed β_0, for the ratio $\delta\beta_{\vec{k}}/\delta\alpha_{\vec{k}}$ vanishes as $k_z \to 0$.

Figure 2 shows the projection of the three-dimensional equilibrium surface (Fig. 1) onto the $\beta_0 - T$ plane, with the region of stability shaded. The solid portion of the marginal stability curve lies on the near side of the ridge in Fig. 1, the dashed portion lies on the far side, and it crosses the ridge near $u \approx 0.67w$, $\beta_0 \approx 0.8$, and $T \approx 0.63T_c$. For $T < 0.5T_c$, the model predicts that the region of stability extends down to $T = 0$ near $u \approx w$ and $\beta_0 \approx \frac{1}{2}\pi$ on the near side, and that a second small region of stability also appears on the far side for $T \lesssim 0.06T_c$ near $u \approx 0$ and $\beta_0 \approx \frac{1}{2}\pi$; since these configurations are experimentally inaccessible, they will not be considered further. In addition, Fig. 2 shows the projection (labeled *a*) of the intersection with the plane $u = u_h \approx 0.721w$. As the sample is cooled through the transition temperature T_h, u presumably assumes this value to minimize the free energy. It then retains this value for $T < T_h$, so that curve *a* represents the locus of equilibrium helices on further cooling. In particular, helical textures should remain stable until $T \approx 0.62T_c$ and $\beta_0 \approx 0.87$, when curve *a* leaves the region of stability. Thus it should be feasible to study stable helices throughout the temperature interval $0.62T_c \lesssim T < T_h \approx 0.82T_c$. Although Fig. 2 shows that stable helices can, in fact, occur at still lower temperatures, it may not be possible to prepare them even if the *A* phase can be supercooled sufficiently, or if the *AB* transition can be suppressed with a magnetic field. This last case involves an additional complication, for the field itself affects the equilibrium form and stability of the helix.[16–19]

The preceding discussion was based on a reasonably realistic model that included the numerically important Fermi-liquid corrections (see the Appendix). Two simpler models were also studied: The first was the weak-coupling gas model without Fermi-liquid corrections, which predicted a behavior similar to that in Figs. 1 and 2, except that the region of stability was narrower and closed off at a finite temperature. Thus the inclusion of Fermi-liquid effects enlarges the stable region for helices, both near the onset T_h and in the unphysical low-temperature domain. The second model considered was the generalized Ginzburg-Landau model, in which $\rho_0/\rho_s^{\parallel}$ replaced T/T_c as the independent variable. The resulting domain for static equilibrium differs qualitatively from Fig. 1, for the two branches (small β_0 and β_0

near $\frac{1}{2}\pi$) remain separate for all $\rho_0/\rho_s^{\parallel}$. Only the small-angle branch has a stable region, and our calculated boundary curve reproduced that found by Kleinert, Lin-Liu and Maki.[7] This agreement serves as a check on the present numerical procedures. On the other hand, the evident difference between the predictions of the generalized Ginzburg-Landau model and the (more realistic) weak-coupling gas model with Fermi-liquid corrections suggests that the former cannot serve as even a qualitative guide to the behavior expected in plausible physical situations.

The preceding analysis treated only three coupled amplitudes $\delta\Phi_{\vec{k}}$, $\delta\alpha_{\vec{k}}$, and $\delta\beta_{\vec{k}}$, and it is important to consider the effect of enlarging the set of trial functions. Motivated by the form of Eq. (49), the basis was extended to include the two "first-harmonic" amplitudes $\delta\Phi_{\vec{k}\pm\vec{u}}$, producing a set of 5 coupled variables. Eliminating the three phase amplitudes $\delta\Phi_{\vec{k}}$, $\delta\Phi_{\vec{k}+\vec{u}}$, and $\delta\Phi_{\vec{k}-\vec{u}}$ leads to a pair of equations for $\delta\alpha_{\vec{k}}$ and $\delta\beta_{\vec{k}}$, whose solution again yields a quadratic equation for the decay constant σ. A numerical analysis similar to that described for the simpler truncation scheme yields essentially identical numerical results with those in Fig. 2. In particular, the instability again occurs in all cases for $\vec{q}=0$ and $\vec{k}=k_z\hat{z}\to 0$. This last fact explains why the two calculations predict equivalent behavior, for the coupling between modes with different $\vec{k}$ vanishes identically at $\vec{q}=0$. Thus the expanded basis (including the amplitudes $\delta\Phi_{\vec{k}\pm\vec{u}}$) turns out to be irrelevant in determining the stability, although the special role of $\vec{q}=0$ could not have been predicted beforehand.

V. DISCUSSION

This paper has analyzed the stability of helical textures in ^{3}He-A in the presence of uniform superflow. The study used Cross's weak-coupling values, including Fermi-liquid corrections, to determine the temperature dependence of the dipole-locked hydrodynamic parameters. As seen in the Appendix, these values differ considerably from those without the Fermi-liquid corrections and from the (still less physical) generalized Ginzburg-Landau model. This work therefore represents the first realistic attempt to study the stability of helical textures in ^{3}He-A. Although the present approximation still omits strong-coupling effects, these are not thought to be important.[13] Thus our calculations should provide a reasonable guide to actual experimental situations. In particular, if weak uniform superflow $w\hat{z}$ can be prepared for T near the onset temperature T_h, then the parameter u would assume a quantized value sufficiently close to the critical value u_h that the resulting helix would be stable throughout an extended range of temperature below T_h. The specific values depend on the Fermi-liquid parameters, but there is no reason to expect qualitative changes in the predictions.

Given the existence of stable helices, it becomes very interesting to consider how they might be detected. One relatively direct approach is to employ probes that are sensitive to l_z. In that case, the change in the apex angle β_0 with decreasing temperature below T_h could yield an unambiguous indication of the onset of helical deformation. Kleinberg has recently reported such an observation with ultrasonic attenuation.[20]

An alternative technique might utilize the anisotropy of the negative-ion mobility[21,22] in superfluid ^{3}He-A to study the effect of the helical texture on the ion's motion. If the ion-mobility tensor is written

$$\mu_{ij}=\mu\delta_{ij}-\mu_0\hat{l}_i\hat{l}_j \tag{51}$$

analogous to that in Eq. (4), it is easy to see that an ion released from rest in a helical texture with an axial field $\vec{E}=E\hat{z}$ will follow a helical trajectory with a spatial period equal to that of the $\hat{l}$ vector ($2\pi/u$) and with a circular projection on the x-y plane of radius

$$r_0=\frac{\mu_0\sin\beta_0\cos\beta_0}{(\mu-\mu_0\cos^2\beta_0)u}\ . \tag{52}$$

Since small u implies a large spatial period, this radius increases for small u because the ion then can move farther in the transverse direction before experiencing the curvature of the helix. Detection of such periodic transverse motion would provide clear evidence for the helical texture and might also allow a direct measurement of the spatial periodicity $2\pi/u$. Typical flow velocities[23] are of order $v_s\approx 10^{-2}$ cm/sec, and the corresponding u_h [see Eq. (41)] has the value $0.7(2m_3v_s/\hbar)\approx 66$ cm^{-1} near T_h. The corresponding spatial period becomes $2\pi/u_h \approx 9\times 10^{-2}$ cm. Furthermore, the anisotropy in the mobility is of order 15%, so that Eq. (52) implies a value $r_0\approx 2\times 10^{-3}$ cm for the radius of the associated circular trajectory.

NMR presents another and very interesting possible approach for studying the helical textures. Since NMR experiments usually employ relatively large magnetic fields ($H\gtrsim 25$ Oe), the magnetic field energy is at least comparable with the dipole energy, and both contributions to the free energy must be considered. For small magnetic fields and small angles β_0, Ref. 16 has studied both the equilibrium configuration and the associated NMR, but the general behavior remains to be investigated. In particular, strong magnetic fields may produce still more complicated periodic textures that could alter the NMR absorption spectrum considerably. Indeed, the induced spin density in the presence of an inhomogeneous texture is known to satisfy a Schrödinger-like equation.[24,25] Thus the NMR in a spatially periodic configuration might have several allowed frequencies,

analogous to the electron bands in a one-dimensional crystal. Such NMR satellites conceivably could explain the observed structure in the flow experiments of Mueller, Flint, and Adams.[23] This possible interpretation is particularly interesting, for it might provide yet another probe that is sensitive to the spatial periodicity of the helix.

A related question is the stability of the uniform texture in more complicated situations involving flow and magnetic fields at arbitrary orientations. Investigation of several special cases has uncovered an instability proportional to $\exp(ik_z z)$ with $\vec{k}$ along the direction of superflow.[16–19] In the large-field limit and with $\vec{H} \| \vec{v}_s$, however, preliminary studies[26] suggest an instability with $\vec{k} \perp \vec{v}_s$, which indicates the importance of allowing for general three-dimensional spatial perturbations. This intriguing problem requires further study, as does the form of the resulting nonuniform equilibrium texture for general magnitude and orientation of $\vec{H}$ and $\vec{v}_s$.

ACKNOWLEDGMENTS

I am grateful to D. J. Bromley and M. R. Williams for helpful comments on a preliminary draft of this paper. Research was sponsored, in part, by the NSF Grant No. DMR 75-08516.

APPENDIX

This Appendix summarizes the studies of the hydrodynamic parameters based on Cross's weak-coupling gas model.[8] Central to all the calculations is the A-phase energy gap $\Delta(T)$, which satisfies the appropriate BCS gap equation.[1,27]

$$\frac{1}{gN(0)} = \frac{3}{2}\int \frac{d\Omega}{4\pi}\sin^2\theta \int_0^{\epsilon_c} d\xi \frac{\tanh\left(\frac{E}{2k_BT}\right)}{E} . \quad \text{(A1)}$$

Here the excitation energy is given by

$$E = (\xi^2 + \Delta^2 \sin^2\theta)^{1/2} , \quad \text{(A2)}$$

and the polar angle θ is measured from the direction $\hat{l}$. The transition temperature has the same value as for an isotropic gap (for example, the B phase of ^{3}He or an s-wave superconductor)

$$k_B T_c = \pi e^{-\bar{\gamma}} \epsilon_c \exp[-1/gN(0)] , \quad \text{(A3)}$$

where $\bar{\gamma}$ is Euler's constant (≈ 0.5772). An expansion of Eq. (A1) near T_c gives the approximate A-phase gap

$$[\Delta(T)]^2 \approx \frac{10}{7\zeta(3)}(\pi k_B T_c)^2 \frac{T_c - T}{T_c} , \quad \text{(A4)}$$

which differs from the isotropic phase by a factor $\frac{5}{4}$. At low temperature, the gap parameter has the form

$$\Delta(T) \approx \Delta_0 \left[1 - \frac{7}{60}\left(\frac{\pi k_B T}{\Delta_0}\right)^4\right] , \quad \text{(A5)}$$

where the zero-temperature limit is given by

$$\Delta_0 = \tfrac{1}{2}\pi \exp(\tfrac{5}{6} - \bar{\gamma}) k_B T_c \approx 2.029 k_B T_c . \quad \text{(A6)}$$

This value exceeds that for an isotropic gap by a factor ≈ 1.15. Furthermore, the algebraic temperature dependence of the correction in Eq. (A5) arises directly from the nodes in the energy gap, in contrast to the exponential temperature dependence familiar in an isotropic superfluid. For intermediate temperatures, Eq. (A1) has been evaluated directly as a double numerical integral. This procedure yields the values shown in Table I, and the corresponding graph is indistinguishable from that found by Combescot.[27]

To proceed with the evaluation of the hydrodynamic parameters, it is next necessary to consider three auxiliary quantities introduced by Cross[8]

$$\alpha(T) = \tfrac{3}{8}\int_0^{\pi/2} d\theta \sin^3\theta \phi(\theta) , \quad \text{(A7a)}$$

$$\beta(T) = \tfrac{3}{2}\int_0^{\pi/2} d\theta \sin\theta \cos^2\theta \phi(\theta) , \quad \text{(A7b)}$$

$$\gamma(T) = 3\int_0^{\pi/2} d\theta \frac{\cos^4\theta}{\sin\theta}\phi(\theta) , \quad \text{(A7c)}$$

TABLE I. Temperature dependence of the parameters used in weak-coupling gas model.

T/T_c	$\Delta(T)/k_BT_c$	$\alpha(T)$	$\beta(T)$	$\gamma(T)$
0.9	1.0411	0.0488	0.0514	0.1623
0.8	1.4105	0.0946	0.1054	0.3538
0.7	1.6492	0.1367	0.1622	0.5842
0.6	1.8113	0.1739	0.2216	0.8686
0.5	1.9185	0.2050	0.2829	1.2316
0.4	1.9834	0.2284	0.3448	1.7154
0.3	2.0160	0.2428	0.4039	2.4011
0.2	2.0275	0.2487	0.4543	3.4663
0.1	2.0297	0.2499	0.4882	5.4440

where

$$\phi(\theta) = 1 - \int_0^\infty d\xi\,(2k_BT)^{-1}\,\mathrm{sech}^2(E/2k_BT) \qquad \text{(A8)}$$

is essentially the Yoshida function.[1] Near T_c, it is straightforward to verify that $\phi(\theta)$ has the form

$$\phi(\theta) \approx \frac{7\zeta(3)}{4}\left[\frac{\Delta}{\pi k_B T_c}\right]^2 \sin^2\theta$$

$$= \tfrac{5}{2}\sin^2\theta\,\frac{T_c - T}{T_c} \quad T \to T_c \qquad \text{(A9)}$$

and Cross's functions have the corresponding limiting behavior

$$\alpha = \beta = \tfrac{1}{3}\gamma \approx \frac{7\zeta(3)}{20}\left[\frac{\Delta}{\pi k_B T_c}\right]^2 = \frac{1}{2}\,\frac{T_c - T}{T_c} \quad T \to T_c\,. \qquad \text{(A10)}$$

At low temperature, in contrast, $\phi(\theta)$ differs from 1 only within an angular interval of order T/T_c near the nodes in the energy gap. An approximate evaluation yields

$$\alpha(T) \approx \tfrac{1}{4}\left[1 - \frac{7}{15}\left(\frac{\pi k_B T}{\Delta_0}\right)^4\right], \qquad \text{(A11a)}$$

$$\beta(T) \approx \tfrac{1}{2}\left[1 - \left(\frac{\pi k_B T}{\Delta_0}\right)^2\right], \qquad \text{(A11b)}$$

$$\gamma(T) \approx 3\ln(T_c/T) - \tfrac{3}{2}\,, \qquad \text{(A11c)}$$

where Eq. (A6) has been used to simplify the last relation. Once again, values for intermediate temperatures were calculated by double numerical integration, with the results shown in Table I.

Given these quantities, it is not difficult to determine the hydrodynamic parameters. In the A phase, for example, direct comparison of Eq. (6) with Cross's expressions omitting Fermi-liquid corrections gives the following identifications:

$$\begin{aligned}
&\rho_s^0 = (K_2)^0 = 4\alpha(\hbar/2m_3)^2\rho\,,\\
&(\rho_s^{\parallel})^0 = 2c^0 = (c_0)^0 = (K_1)^0 = 2\beta(\hbar/2m_3)^2\rho\,,\\
&(\bar{K}_s)^0 = \alpha(\hbar/2m_3)^2\rho\,, \qquad \text{(A12)}\\
&(\bar{K}_t)^0 = \tfrac{1}{3}(\alpha + 2\beta)(\hbar/2m_3)^2\rho\,,\\
&(\bar{K}_b)^0 = (\beta + \tfrac{2}{3}\gamma)(\hbar/2m_3)^2\rho\,,
\end{aligned}$$

where the superscript 0 denotes the value without Fermi-liquid correction and the bar denotes the value without dipole locking. In this approximation, we note that $(\rho_s^{\parallel})^0 = (c_0)^0$ at all temperatures, and that the relative anisotropy in the superfluid density tensor may be written

$$\left(\frac{\rho_0}{\rho_s^{\parallel}}\right)^0 = \frac{2\alpha - \beta}{\beta}\,. \qquad \text{(A13a)}$$

It falls monotonically from 1 at T_c and has the following low-temperature behavior:

$$\left(\frac{\rho_0}{\rho_s^{\parallel}}\right)^0 \approx \left(\frac{\pi k_B T}{\Delta_0}\right)^2, \quad T \ll T_c\,. \qquad \text{(A13b)}$$

These temperature-dependent quantities are shown in Figs. 3–6.

The inclusion of Fermi-liquid corrections is straightforward, for they involve only odd-l Landau parameters and the temperature-dependent functions

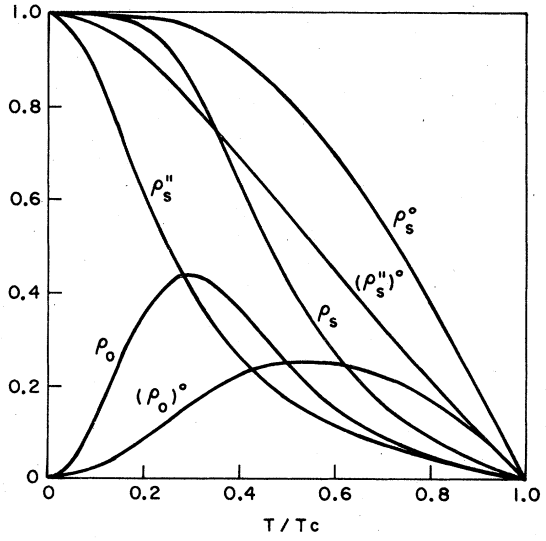

FIG. 3. Elements of the superfluid density tensor calculated with the weak-coupling gas model, in units of $\rho(\hbar/2m_3)^2$. The superscript 0 indicates the value without Fermi-liquid corrections.

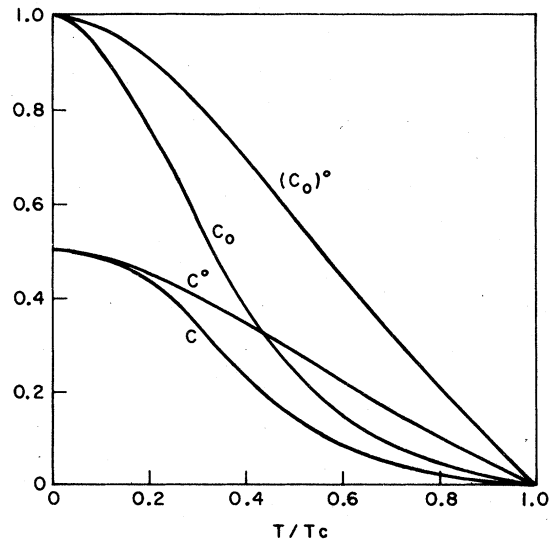

FIG. 4. Elements of the tensor $\bar{c}$ calculated with the weak-coupling gas model in units of $\rho(\hbar/2m_3)^2$. The superscript 0 indicates the value without Fermi-liquid corrections.

α, β, and γ. In this way, for example, the hydrodynamic parameters in f_k become

$$\rho_s = 4\frac{1+\frac{1}{3}F_1^s}{1+\frac{1}{3}F_1^s(1-4\alpha)}\frac{m}{m^*}\alpha\left(\frac{\hbar}{2m_3}\right)^2\rho = \frac{(\rho_s)^0}{1+\frac{1}{3}F_1^s(1-4\alpha)},$$

$$\rho_s^{\parallel} = 2\frac{1+\frac{1}{3}F_1^s}{1+\frac{1}{3}F_1^s(1-2\beta)}\frac{m}{m^*}\beta\left(\frac{\hbar}{2m_3}\right)^2\rho = \frac{(\rho_s^{\parallel})^0}{1+\frac{1}{3}F_1^s(1-2\beta)}, \tag{A14}$$

$$c = \frac{1+\frac{1}{3}F_1^s}{1+\frac{1}{3}F_1^s(1-4\alpha)}\frac{m}{m^*}\beta\left(\frac{\hbar}{2m_3}\right)^2\rho = \frac{c^0}{1+\frac{1}{3}F_1^s(1-4\alpha)}, \qquad c_0 = c+\tfrac{1}{2}\rho_s^{\parallel},$$

where $m^*/m = 1+\frac{1}{3}F_1^s$. For specific numerical work, I have followed Cross in using the approximate values $\frac{1}{3}F_1^s = 5.22$ and $\frac{1}{3}F_1^a = -0.18$. The resulting quantities are shown in Figs. 3 and 4, in comparison with the values omitting Fermi-liquid corrections. Near T_c, the only effect of these corrections is the overall reduction factor m/m^*, which decreases the hydrodynamic parameters considerably. At zero temperature, in contrast, the denominators in Eq. (A14) all reduce to 1, reproducing the uncorrected values. Note, particularly, that c_0 typically differs from $\rho_s^{\parallel}$, and that ρ_0 exceeds $\rho_s^{\parallel}$ for $T \gtrsim 0.3T_c$. Thus the Fermi-liquid effects enhance the anisotropy in the superfluid density tensor throughout the whole A phase. This last observation indicates that the generalized Ginzburg-Landau approximation cannot be accurate even near T_c, for the ratio $\rho_0/\rho_s^{\parallel}$ actually increases with decreasing temperature reaching the value ≈ 1.44 at $T \approx 0.5T_c$.

In a similar way, the bending constants become

$$\bar{K}_s = \frac{m}{m^*}(\bar{K}_s)^0,$$

$$\bar{K}_t = \frac{m}{m^*}\left[(\bar{K}_t)^0 + \frac{\frac{1}{3}F_1^s}{1+\frac{1}{3}F_1^s(1-2\beta)}\beta^2\left(\frac{\hbar}{2m_3}\right)^2\rho\right],$$

$$\bar{K}_b = \frac{m}{m^*}\left[(\bar{K}_b)^0 + \frac{\frac{1}{3}F_1^s}{1+\frac{1}{3}F_1^s(1-4\alpha)}\beta^2\left(\frac{\hbar}{2m_3}\right)^2\rho\right],$$

$$K_1 = \frac{m}{m^*}\frac{1+\frac{1}{3}F_1^a}{1+\frac{1}{3}F_1^a(1-2\beta)}(K_1)^0, \tag{A15}$$

$$K_2 = \frac{m}{m^*}\frac{1+\frac{1}{3}F_1^a}{1+\frac{1}{3}F_1^a(1-4\alpha)}(K_2)^0,$$

where the dipole-locked values follow directly from

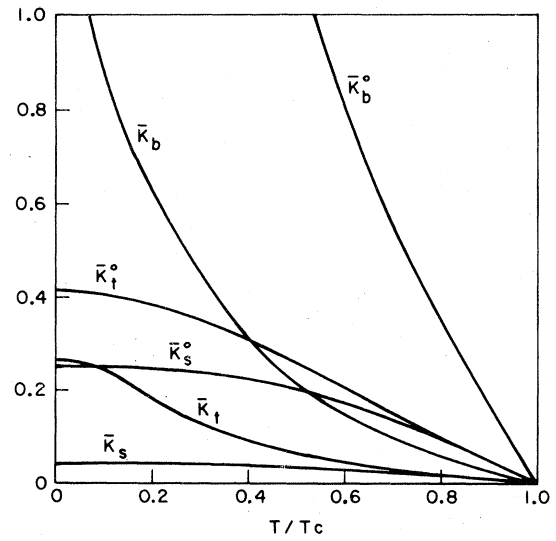

FIG. 5. Unlocked bending constants calculated with the weak-coupling gas model in units of $\rho(\hbar/2m_3)^2$. The superscript 0 indicates the value without Fermi-liquid corrections.

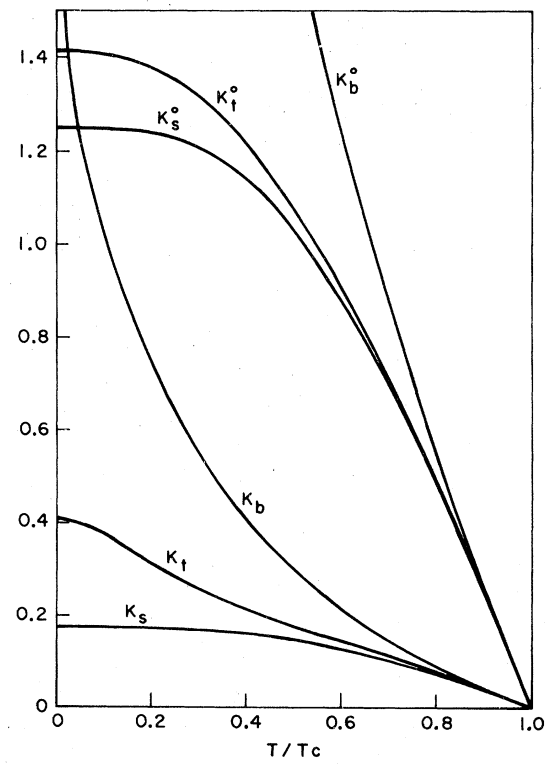

FIG. 6. Dipole-locked bending constants calculated with the weak-coupling gas model in units of $\rho(\hbar/2m_3)^2$. The superscript 0 indicates the value without Fermi-liquid corrections.

Eq. (10). Unlike the previous hydrodynamic parameters, the Fermi-liquid corrections here suppress these quantities at all temperatures, as seen in Figs. 5 and 6 for both the unlocked and locked cases. Since the onset temperature T_h for the appearance of a helical deformation in zero magnetic field is determined by the condition $\rho_0 K_b = (c_0 + \frac{1}{2}\rho_s^{\parallel})^2$, it is not immediately evident how the corrections will affect T_h. With the present choice of Landau parameters, I find $T_h^0 = 0.88\,T_c$ without corrections and $T_h = 0.82\,T_c$ with them, so that the net effect is actually to stabilize the uniform texture.

---

[1]A. J. Leggett, Rev. Mod. Phys. 47, 331 (1975).
[2]J. C. Wheatley, Rev. Mod. Phys. 47, 415 (1975).
[3]P. Bhattacharyya, T.-L. Ho, and N. D. Mermin, Phys. Rev. Lett. 39, 1290 (1977).
[4]J. R. Hook and H. E. Hall, (unpublished); J. R. Hook, J. Phys. (Paris) 39, C6-17 (1978).
[5]M. C. Cross and M. Liu, J. Phys. C 11, 1795 (1978).
[6]A. L. Fetter, Phys. Rev. Lett. 40, 1656 (1978); J. Phys. (Paris) 39, C6-46 (1978).
[7]H. Kleinert, Y. R. Lin-Liu, and K. Maki, J. Phys. (Paris) 39, C6-59 (1978); Phys. Lett. A 70, 27 (1979).
[8]M. C. Cross, J. Low Temp. Phys. 21, 525 (1975).
[9]P. G. de Gennes, *The Physics of Liquid Crystals* (Oxford University, London, 1974), Chap. 3.
[10]See, for example, A. R. Edmonds, *Angular Momentum in Quantum Mechanics* (Princeton University, Princeton, N. J., 1957), p. 6.
[11]M. C. Cross and P. W. Anderson, in *Proceedings of the Fourteenth International Conference on Low Temperature Physics,* edited by M. Krusius and M. Vourio (North-Holland, Amsterdam, 1976), Vol. I, p. 29.
[12]W. F. Brinkman and M. C. Cross, in *Progress in Low Temperature Physics,* edited by D. J. Brewer (North-Holland, Amsterdam, 1978), Vol. VII.
[13]J. W. Serene and D. Rainer, Phys. Rev. B 17, 2901 (1978).
[14]See, for example, A. L. Fetter and J. D. Walecka, *Theoretical Mechanics of Particles and Continua* (McGraw-Hill, New York, to be published), Chap. IV.
[15]D. N. Paulson, M. Krusius, and J. C. Wheatley, Phys. Rev. Lett. 37, 599 (1976).
[16]Y. R. Lin-Liu, K. Maki, and D. Vollhardt, J. Phys. Lett. (Paris) 39, L-381 (1978).
[17]W. M. Saslow and C.-R. Hu, J. Phys. Lett. (Paris) 39, L-379 (1978).
[18]S. Takagi (unpublished).
[19]H. Kleinert (unpublished).
[20]R. L. Kleinberg, Phys. Rev. Lett. 42, 182 (1979).
[21]A. I. Ahonen, J. Kokko, O. V. Lounasmaa, M. A. Paalanen, R. C. Richardson, W. Schoepe, and Y. Takano, J. Low Temp. Phys. 30, 205 (1978).
[22]P. D. Roach, J. B. Ketterson, P. R. Roach, Phys. Rev. Lett. 39, 626 (1977).
[23]H. Smith, W. F. Brinkman, and S. Engelsberg, Phys. Rev. B 15, 199 (1977).
[24]L. J. Buchholtz, Phys. Rev. B 18, 1107 (1978).
[25]R. M. Mueller, E. B. Flint, and E. D. Adams, Phys. Rev. Lett. 36, 1460 (1976); E. B. Flint, R. M. Mueller, and E. D. Adams, J. Low Temp. Phys. 33, 43 (1978).
[26]A. L. Fetter and M. R. Williams (unpublished).
[27]R. Combescot, J. Low Temp. Phys. 18, 537 (1975).